

ORIGINAL ARTICLE

Ultrahigh-gain single SnO₂ nanowire photodetectors made with ferromagnetic nickel electrodes

Meng-Lin Lu^{1,2}, Tong-Min Weng^{1,2}, Ju-Ying Chen¹ and Yang-Fang Chen¹

We report the first attempt at magnetic manipulation of the photoresponse in a one-dimensional device in which a highly sensitive ultraviolet photodetector, composed of tin dioxide nanowire (SnO₂ NW) and ferromagnetic nickel (Ni) electrodes, has been fabricated and characterized. Surprisingly, as the Ni electrodes were magnetized, the photocurrent gain was greatly enhanced by up to 20 times, which is far beyond all of the previously reported enhancement factors for functionalized NW photodetectors. The underlying mechanism enabling the enhanced gain is attributed to both oxygen molecules adsorbed and surface band-bending effects due to the migration of electrons to the surface of SnO₂ NW caused by the magnetic field of ferromagnetic electrodes. The novel approach presented here can provide a new route for the creation of highly efficient optoelectronic devices based on the coupling between ferromagnetic materials and nanostructured semiconductors.

NPG Asia Materials (2012) 4, e26; doi:10.1038/am.2012.48; published online 14 September 2012

Keywords: ferromagnetic material; SnO₂ nanowire; ultrahigh-gain photodetector

INTRODUCTION

It is well known that the magnetization produced by ferromagnetic materials can be used to control the charge carrier flow in a nearby substrate, which serves as a fundamental process underlying many current technologies.^{1,2} However, the literature on the integration of ferromagnetic materials into nanoscale semiconductor devices is rather limited.³ One-dimensional metal-oxide semiconductor nanostructures have been extensively investigated in the past because of their unique characteristics and broad potential for various applications.^{4,5} In fact, a variety of optoelectronic devices based on one-dimensional nanowires (NWs) have been developed, such as emitters,^{6,7} detectors^{8,9} and transistors.^{10,11} Recently, tin dioxide (SnO₂) with a wide direct band gap of 3.6 eV and high quantum efficiency in the ultraviolet region has attracted a great deal of attention, and there are potential applications in many practical devices, such as visible-blind photodetectors and solar cells.^{12–15} In addition, because NWs have a high surface-to-volume ratio, the surface of NWs can influence the conductivity markedly. Owing to charged defects located at SnO₂ NWs surface, the upward band-bending forms a low-conductivity depletion layer. Once electron-hole pairs are photoexcited, holes will drift to the surface through the electric field, leaving unpaired electrons inside; thus, the recombination probability of electrons and holes reduces, and the lifetime of photo-generated carriers increases.^{16,17} SnO₂ NWs therefore have been developed to detect gas molecules, including CO, NO₂, and so on^{18,19} because the adsorbed gas molecules on the surface will extract charge carriers from SnO₂ and react with adhered gas, resulting in

altered conductivity. To improve the sensitivity of the devices, SnO₂ NW has been functionalized with several different materials including catalytically active metals, p-type semiconductors, and semiconductor quantum dots.^{20–24} Through these previous efforts, the photocurrent (PC) gain of SnO₂ NW devices can be not only greatly enhanced but also extended to a wider photoresponse spectrum range. In this paper, we provide an alternate approach to enhance the sensitivity of a single SnO₂ NW photodetector that has two ferromagnetic nickel (Ni) electrodes. Our strategy is the first attempt at magnetic manipulation of photoresponse in a one-dimensional semiconductor device. Quite surprisingly, the enhancement factor ratio for magnetic to nonmagnetic electrode-containing devices exceeds 20 times, which is much larger than all of the previously reported values for semiconductor NW photodetectors. The underlying mechanism is interpreted in terms of the migration of electrons to the NW surface due to magnetized Ni electrodes, which will enhance both oxygen adsorbed and surface band-bending effects and lead to the amplification of PC gain. The results we describe here could therefore open up a new route for the creation of high-efficiency optoelectronic devices based on the coupling between ferromagnetic materials and nanostructured semiconductors.

EXPERIMENTAL PROCEDURES

The growth of SnO₂ NWs is based on a vapor–liquid–solid process. In the synthesis process, an Au layer of 10 nm thickness was first deposited on M-plane (100) sapphire (Al₂O₃) to serve as the catalyst. Then, Sn powder was placed on a ceramic boat and put in a furnace with argon flow as a carrier gas

¹Department of Physics, National Taiwan University, Taiwan, Taipei, Republic of China

Correspondence: Professor Y-F Chen, Department of Physics, National Taiwan University, Taiwan, Taipei 106, Republic of China.

E-mail: yfchen@phys.ntu.edu.tw

²These authors contributed equally to this work.

Received 24 May 2012; revised 27 July 2012; accepted 27 July 2012

at a flow rate of 200 sccm. The temperature was increased from room temperature to 1000 °C at a rate of 100 °C min⁻¹. After a growth time of 5 min at 1000 °C, the SnO₂ NWs were obtained. To reduce surface defects, the as-grown NWs were annealed at 1000 °C for 3 h. Figure 1a shows the field emission scanning electron micrograph image of the morphology of SnO₂ NWs obtained by a JSM-6500F field emission scanning electron micrograph system (JEOL Ltd, Tokyo, Japan). The X-ray diffraction analysis of SnO₂ NWs was carried out using a diffractometer (Panalytical X'pert PRO, PANalytical, Almelo, Netherlands) with K α line as the incident radiation; X-ray diffraction is used to identify the structure of synthesized product. Most of the peaks can be perfectly indexed according to the tetragonal rutile structure of SnO₂, as shown in the inset of Figure 1a. The transmission electron microscopy images of as-grown NWs and annealed NWs are shown in Figures 1b and c, respectively. We can clearly observe that the surface of the annealed NWs is smoother than that of the as-grown NWs.²⁵

After the fabrication, the SnO₂ NWs devices were made by the shadow-mask method,¹³ and Ni (200 nm)/Au (20 nm) electrodes were deposited on the SnO₂ NWs to form ohmic contacts. A typical SEM image of a single SnO₂ NW device is illustrated in Figure 1d. The distance of the channel between two terminals is 8 μ m, and the diameter of the NW is ~50 nm. A thermal annealing at 500 °C for 15 s after contact deposition was necessary to minimize the contact resistance. In our work, an external magnetic field provided by a pair of electromagnets is applied in the normal direction of the plane of the substrate. After the electrodes were magnetized, the NW device was transferred onto a stage under the microscope without external magnetic field. For the PC measurement, a He–Cd laser working at 325 nm was used as the excitation light source. A Keithley 236 measurement system (Keithley Instrument, Inc., Cleveland, OH, USA) was used to supply the dc voltage (0.1 V) and to record the PC.

RESULTS AND DISCUSSION

Figure 2 shows the dark currents of the device after the Ni electrodes were magnetized under different magnetic fields. We can clearly see that the dark current decreases with increasing magnetic field. This phenomenon of decreased dark current with increasing magnetic field can be understood as follows: when free electrons flow through the

conducting channel of the NW, the electrons migrate to the surface of NW due to the Lorentz force caused by the magnetic field and trapped by the surface defects, the number of conducting electrons is therefore reduced and the resistance of NW increases. Moreover, the electron accumulation at the NW surface generates a depletion region near the surface of NW and a high-resistance zone is formed, which further increases the resistance of NW. When the magnetic field increases, the amount of the accumulated electrons is larger, and thus, the high-resistance zone near the surface of NW also becomes larger.^{22,23} To be more quantitative, let us consider the Hall effect. The value of the Hall electric field E_B can be expressed as $|\vec{v}_d \times \vec{B}_d|$, where \vec{v}_d is the drift velocity, and \vec{B}_d the magnetic field. As the

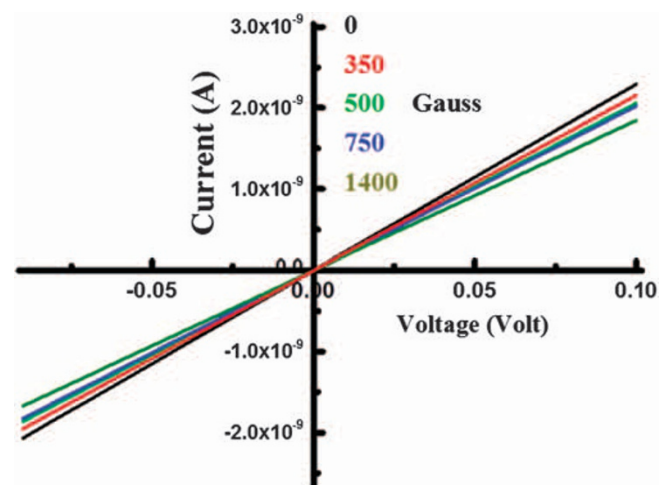


Figure 2 I – V characteristics of a single SnO₂ nanowire (NW) device exposed to different magnetic field strengths.

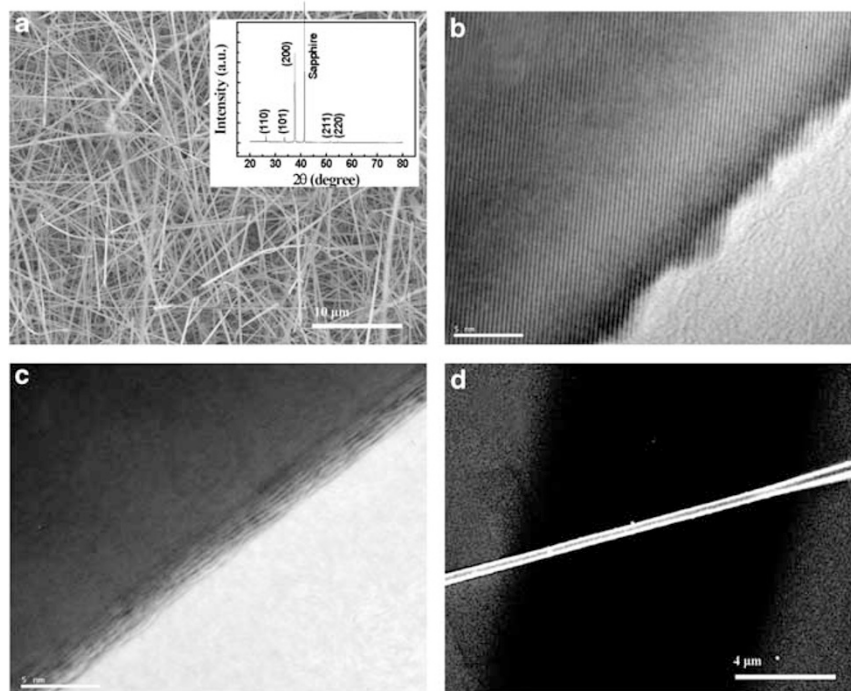


Figure 1 (a) Field emission scanning electron microscope (FE-SEM) image of as-grown SnO₂ nanowires (NWs). Inset: X-ray diffraction (XRD) pattern of as-grown SnO₂ NWs. (b) Transmission electron microscopy (TEM) image of as-grown SnO₂ NW. (c) TEM image of annealed SnO₂ NW. (d) SEM image of single SnO₂ NW device. The distance of the channel between two terminals is 8 μ m, and the diameter of the NW is ~50 nm.

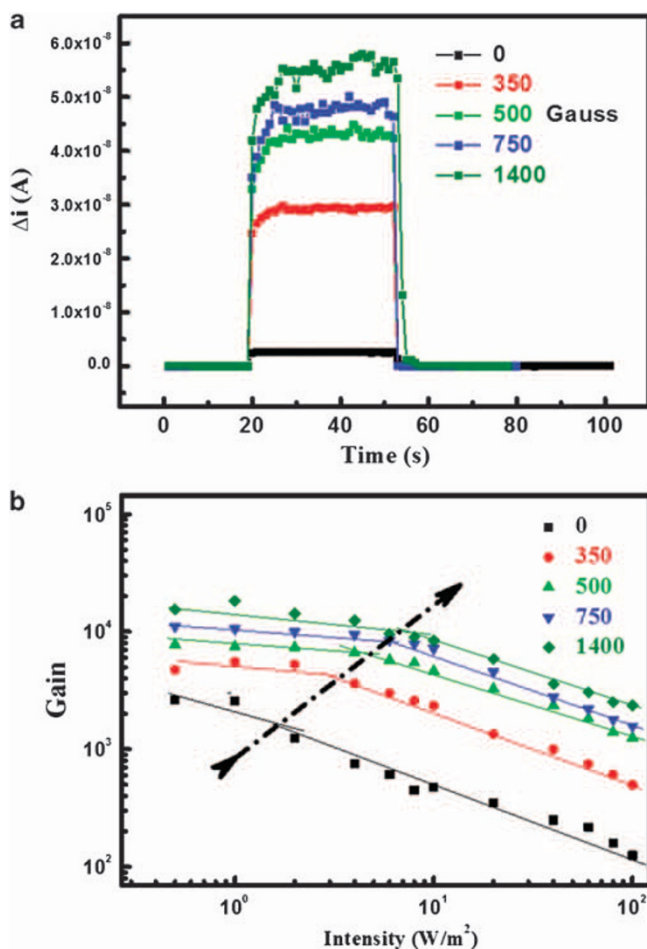


Figure 3 (a) Photoresponse of a single SnO₂ nanowire (NW) device with a bias of 0.1 V exposed to magnetic field strengths of 350, 500, 750 and 1400 G and the illumination of a He–Cd laser working at 325 nm with an excitation intensity of 8 W m⁻². (b) The gain logarithmic plot versus illumination intensity of a single SnO₂ NW device exposed to magnetic field strengths of 350, 500, 750 and 1400 G.

number of accumulated charges is proportional to E_B , the dark current therefore decreases with increasing magnetic field. In addition, we have performed a similar experiment for the magnetic field parallel to the axis of NW. In this case, the current does not change with increasing magnetic field. This lack of change in conductivity with a parallel magnetic field therefore provides additional evidence to support our interpretation. A more detailed examination of the decrease of dark current with increasing magnetic field is also discussed in a later section. Upon illumination with photon energy larger than the energy band gap of SnO₂ (3.6 eV), the conductivity of SnO₂ NWs increases greatly due to photo-generated electron–hole pairs. As shown in Figure 3a, the photoresponse of an NW device with a bias of 0.1 V under the illumination of He–Cd laser (325 nm) with the excitation intensity of 8 W m⁻² can be clearly observed. Surprisingly, after the Ni electrodes were magnetized, the PC is greatly enhanced. For instance, the PC difference ($\Delta i = i_{\text{light}} - i_{\text{dark}}$) of the NW device can be enhanced by 590%, 1200%, 1750% and 2100%, as the electrodes were magnetized under the field of 350, 500, 750 and 1400 G, respectively.

Here, we investigate the PC gain of this NW photodetector with the magnetized electrodes. The current gain (Γ) of the photoresponse,

a factor used to determine the efficiency of electrons induced by photon and collected during the PC measurement can be calculated using the expression¹³

$$\Gamma = \frac{\Delta i/q}{P/h\nu} \times \frac{1}{\eta}, \quad (1)$$

where Δi is the current difference between the PC and dark current, q is the electron charge, $h\nu$ is the photon energy of the incident light, P is the power of photon that the NW has absorbed and is expressed by $P = I \times l \times d$ and I is the excitation intensity illuminating on the pattern, l and d are the length and the width of the NW, respectively, and η is the quantum efficiency, which is set to 1 for simplicity because the magnitude rather than absolute value is emphasized. Without a magnetic field, the calculated PC gain of the single SnO₂ NW device is ~ 2500 at an intensity of 1 W m⁻² under He–Cd laser (325 nm) illumination. We then calculate the gain achieved by different magnetic fields caused by ferromagnetic electrodes. Quite interestingly, the gain of the photodetector can reach up to almost 20 000 when the electrodes are magnetized in a field of 1400 G. Compared with the PC gain for the unmagnetized electrodes, the enhancement factor is estimated to be 800%. According to the data shown in Figure 3b, the highest enhancement factor can even exceed 2000%. This value is much larger than all of the previously reported enhancement factors for functionalized NW photodetectors, as summarized in Table 1.^{26–28} Therefore, it is very desirable to understand the mechanism enabling the ultrahigh PC gain obtained here.

According to the reports by Binet *et al.*²⁹ and Muñoz *et al.*³⁰ the relationship between the PC gain and the illumination intensity is very informative when considering the underlying mechanism. As shown in Figure 3b, the gain plot (logarithmic) versus intensity shows that there is a turning point in each curve and that the value of the light intensity for the turning point to occur increases with increasing magnetization of the ferromagnetic electrodes. First, the existence of a critical value of turning point is considered. For the excitation intensity below the critical value, Γ versus intensity follows an inverse power law (that is, $\Gamma \propto I^{-\kappa}$), and the value of the exponent κ is ~ 0.1 – 0.2 . According to the theoretical work of the κ value reported previously, the behavior in this regime can be understood in terms of oxygen-related hole-trap filling mechanism.³¹ More explicitly stated, when the NW is exposed in air and adsorbs oxygen molecules at its surface, the adsorbed oxygen molecules will capture electrons from the NW and become negatively charged. This relationship can be described by the expression:



Under the light illumination, the photoinduced holes will migrate to the surface owing to the surface electric field and discharge negative-charged oxygen molecules, as described by the expression:



The neutralized oxygen molecules are photodesorbed from the surface. Therefore, the presence of hole-trap states will prolong the photoinduced electron lifetime, and thus, the gain can be amplified.

Once the excitation intensity exceeds the critical value, oxygen-related hole-trap states will be filled, which will change the electron–hole recombination behavior.¹³ At intensities exceeding the critical value of the turning point, the value of the exponent κ increases to a value of 0.6–0.8 as calculated from Figure 3b. Based on theoretical

Table 1 Comparison of the enhancement factor for 1D inorganic semiconductor NW-photodetectors obtained in the present work and previous reports

Photodetectors	Original	After functionalization	Enhancement factor (%)	Ref.
Au-coated SnO ₂ NW	115 (10 W m ⁻²)	140	121.7	22
NiO-decorated SnO ₂ NW	800 (8 W m ⁻²)	1300	162.5	23
CdSe QDs-decorated SnO ₂ NW	1500 (8 W m ⁻²)	4000	266.7	24
Piezoelectric effect assisted ZnO NW	—	—	530	26
			(Max value)	
Au-coated ZnO NW	1.4 × 104 (0.62 W m ⁻²)	2.8 × 10 ⁴	200	27
Present work	^a 2.5 × 10 ³ (1 W m ⁻²) ^a 450 (8 W m ⁻²) ^b 8.8 × 10 ³ (0.5 W m ⁻²) ^b 750 (8 W m ⁻²) ^c 2 × 10 ⁴ (1 W m ⁻²) ^c 2.4 × 10 ³ (10 W m ⁻²)	2.0 × 10 ⁴ 9.1 × 10 ³ 4.7 × 10 ⁴ 2.2 × 10 ⁴ 9.1 × 10 ⁴ 4.9 × 10 ⁴	800 2023 534 2933 450 2008	—

Abbreviations: NW, nanowire; QD, quantum dot; 1D, one-dimensional.

^aAnnealed single SnO₂ NW with magnetized Ni electrodes.

^bAs-grown single SnO₂ NW under the growth time of 5 min with magnetized Ni electrodes.

^cAs-grown single SnO₂ NW under the growth time of 1 min with magnetized Ni electrodes.²⁸

investigations,^{30–33} the PC gain is now dominated by the modulation of surface space charge region (SCR).³⁰ The existence of oxygen vacancies on the surface of an SnO₂ NW causes the accumulation of free electrons on the NW surface.³² Consequently, the low-conductivity depletion region near the surface, referred to as SCR, is formed because of the existence of the upward band bending. Once electron–hole pairs are photogenerated, the photoinduced holes drift to the surface readily due to the built-in electric field, leaving unpaired electrons inside; thus, photogenerated electrons and holes are spatially separated. The spatial separation of electrons and holes reduces the electron–hole recombination rate; therefore, the electron lifetime is increased, and the photoresponse is enhanced. According to the simulation by Garrido *et al.*,³³ the exponent κ of the PC induced by the modulation of surface SCRs is between 0.5 and 0.9, which is in good agreement with our experimental measurements.

Next, we discuss the gain behavior under the magnetic field caused by the magnetized Ni electrodes with the magnetization in the direction normal to the substrate plane. As the current flows through the conducting channel of NW, the electrons will migrate to the surface of NW due to the Lorentz force, and then, the amount of oxygen adsorbed by NW will be increased. Under this circumstance, not only is the oxygen-related hole-trapping effect enhanced but also the surface band bending becomes more pronounced, as illustrated in Figure 4. Therefore, the pumping intensity that is needed to transfer the PC gain from the hole-trap filling to SCR mechanism will increase, and the critical value of the turning point therefore becomes larger when the strength of the magnetic field increases.

To support the above interpretation, a more detailed examination of the behavior caused by Ni electrodes has been performed. Figure 5a shows the hysteresis curves of an Ni thin film exposed to an external magnetic field with the direction normal to the plane of the sample.^{34,35} The hysteresis loops show that a larger remanence magnetization (m_r) can be obtained with a higher maximum of external field (B_{max}). As shown in Figure 5b, the relationship between m_r and B_{max} can be fit with a logarithmic function, that is, $m_r \propto \log(B_{max})$. We now examine the correlation of the decrease of dark current with increasing m_r . In the model of oxygen molecules

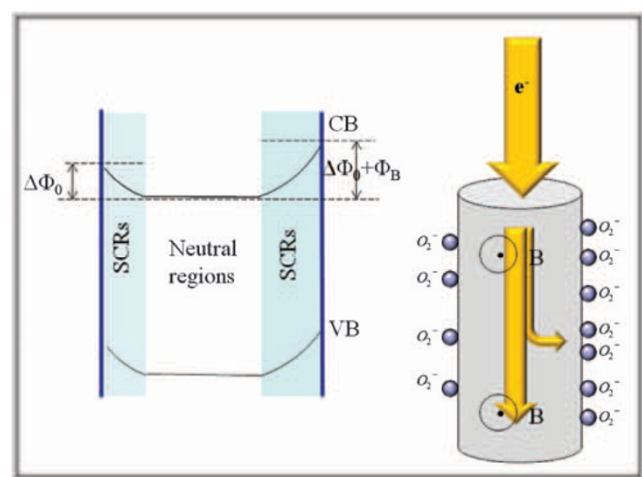


Figure 4 Photocurrent gain mechanism of both oxygen-related hole trapping and surface band-bending effects with the assistance of magnetic field.

detection, the dependence of the resistance of NW (R_{NW}) on the oxygen partial pressure ($p(O_2)$) can be expressed as follows:^{36,37}

$$R_{NW} \propto p(O_2)^n \quad (4)$$

In our case, the oxygen partial pressure surrounding the NW surface is proportional to the number of electrons accumulated on the NW surface, and the number of accumulated electrons is also proportional to the magnetic field generated by m_r as described above. Thus, a simple relationship can be drawn as follows:

$$R_{NW} \propto p(O_2)^n \propto m_r^n \quad (5)$$

According to the previous report, the exponent n has a value of 1/4 at room temperature.³⁷ As shown in Figure 6, the exponent $n \approx 1/4$ can be used to fit our experiment data quite well in the low m_r region. However, in the high m_r region, the exponent deviates from 1/4 very significantly, which can be explained as follows. The conductivity of

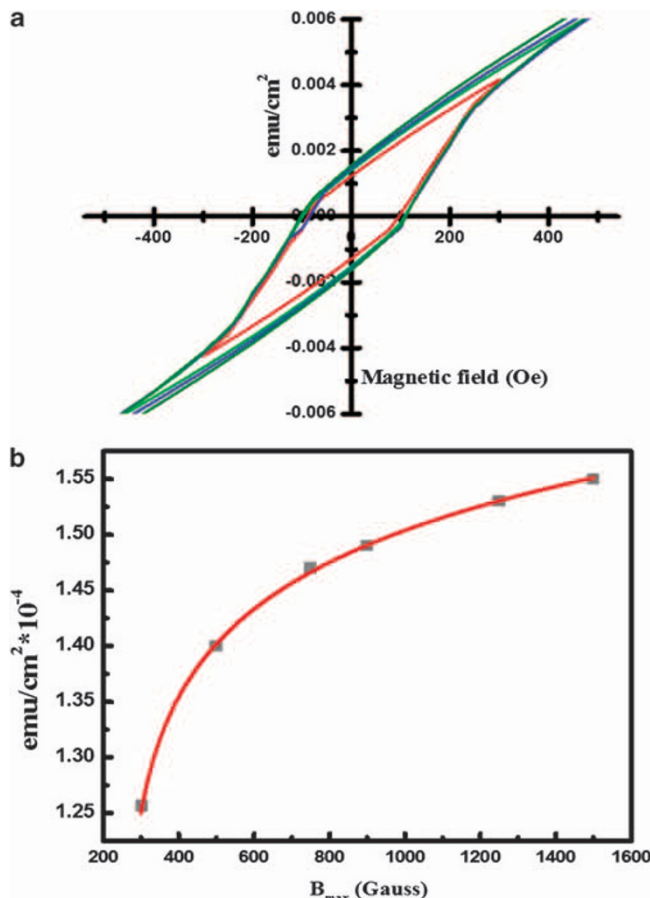


Figure 5 (a) Hysteresis curves of nickel (Ni) thin film with the direction of external magnetic field perpendicular to the plane of the sample. (b) Remanence magnetization (m_r) plot versus the maximum of external field (B_{\max}).

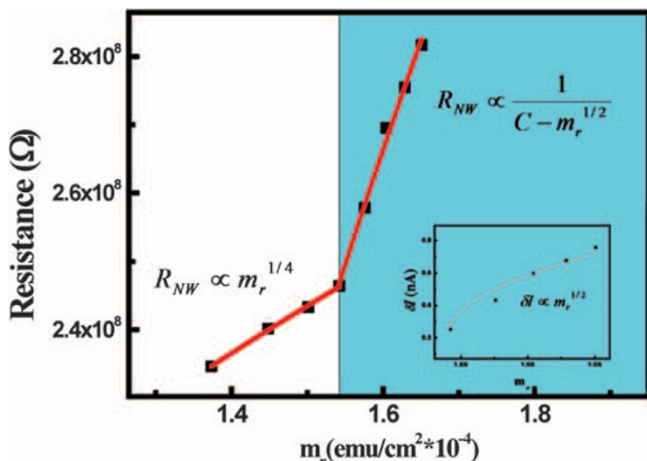


Figure 6 Resistance of nanowire (NW) (R_{NW}) plot versus remanence magnetization (m_r). R_{NW} is proportional to $m_r^{1/4}$ at low m_r region, and R_{NW} is proportional to $\frac{1}{C - m_r^{1/2}}$ at high m_r region. Inset: the current difference with and without magnetic field (δI) is proportional to $m_r^{1/2}$.

NW is now dominated by the SCRs mechanism.³³ The current difference (δI) with and without magnetic field can be expressed as follows:

$$\delta I = \frac{i_{\text{without}}}{d - w_{\text{without}}} \times \left\{ \left[\frac{2\epsilon(\Delta\Psi_0 + \Psi_B)}{qN_d} \right]^{1/2} - \left[\frac{2\epsilon\Delta\Psi_0}{qN_d} \right]^{1/2} \right\}, \quad (6)$$

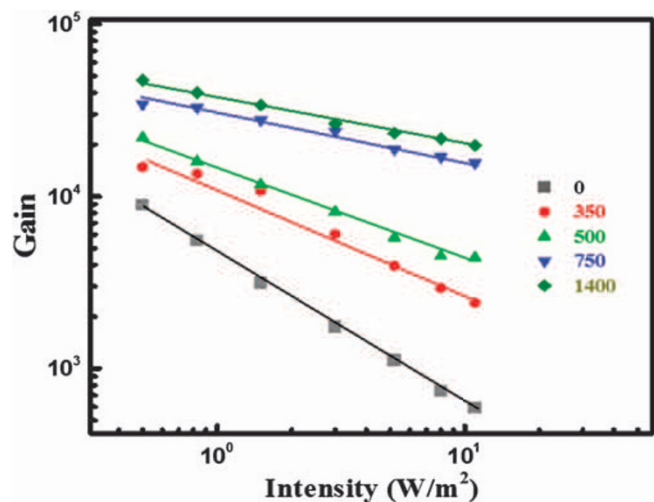


Figure 7 The gain logarithmic plot versus illumination intensity of as-grown single SnO₂ nanowire exposed to magnetic field strengths of 350, 500, 750 and 1400 G.

where

$$w_{\text{without}} \approx \left(\frac{2\epsilon\Delta\Psi_0}{qN_d} \right)^{1/2} \quad (7)$$

$\Delta\Psi_0$ is the intrinsic barrier height, ϵ is the permittivity, N_d is the doping level, $V_T = kT/q$, A is Richardson constant = $1.2 \times 10^6 \text{ A m}^{-2} \text{ K}^{-2}$ and Ψ_B is the barrier height induced by the magnetic field with a linear relationship. Thus, the correlation between δI and m_r can be expressed as $\delta I \propto m_r^{1/2}$. As shown in the inset of Figure 6, our measurements can be described well by the above expression. Furthermore, a more careful examination shows δI is equal to $i_{\text{without}} - i_{\text{measured}} = V/(R_{\text{without}} - R_{\text{NW}})$, where V is the applied bias. Thus, the relationship between R_{NW} and m_r can be expressed as follows:

$$R_{\text{NW}} = \frac{V}{\frac{1}{R_{\text{without}}} - \delta I} \propto \frac{1}{C - m_r^{1/2}}, \quad (8)$$

where C is a constant. The experimental data shown in Figure 6 indicates that the fitting curve is also in good agreement with the above theoretical prediction. Therefore, all of the novel properties observed in our measurements induced by the magnetized Ni electrodes can be well understood, including the decrease of dark current, the occurrence of the critical point as well as ultrahigh gain phenomenon.

Finally, an additional experiment of PC gain versus light intensity has also been performed for the as-grown NW device, as shown in Figure 7. The PC gain of the device without the assistance of magnetic field can reach up to 8800 due to more surface defects than that of the annealed NW device.³⁸ With the effect of the magnetized Ni electrodes, the PC gain can be as high as 4.7×10^4 , and the highest enhancement factor can also have a large value of 3000%. This result demonstrates that the ultrahigh gain phenomenon can also be obtained even if the pristine NWs have a higher state of surface defects. It is worth noting that a very high-gain value up to 10^7 on SnO₂ NW photodetector has been reported previously.³⁹ However, in that case, the ultrahigh gain phenomenon was observed with an electrode separation of $\sim 2 \mu\text{m}$ under an external bias of 1 V. Those experimental conditions are quite different from ours. In our study, the electrode separation is $8 \mu\text{m}$, and the external bias is 0.1 V.

For a fair comparison, we should examine the definition of PC gain in detail. The current gain can also be expressed as follows:¹³

$$\Gamma = \frac{\tau_{\text{life}}}{t} = \tau_{\text{life}} \times \mu \times \frac{V}{l^2}, \quad (9)$$

where τ_{life} is excess carrier lifetime, t is the transit time of the carrier between electrodes, μ is carrier mobility, V is applied bias and l is the distance between electrodes. Based on the same experimental condition, the calculated gain value for our as-grown SnO₂ NW can be up to 3.2×10^6 . With the Ni electrodes, a gain value of up to 1.5×10^7 can be reached, which is comparable to the ultrahigh gain reported previously.³⁹ Therefore, there is no doubt that an ultrahigh enhancement factor can be achieved in our devices under conditions similar to previous experiments.

CONCLUSION

In summary, ultrahigh gain in photodetectors based on single SnO₂ NWs with ferromagnetic Ni electrodes has been demonstrated. The underlying mechanisms are attributed to both oxygen-related hole-trapping and surface band-bending effects induced by the magnetized ferromagnetic electrodes. The PC gain value can be enhanced by >2000% compared with that of the devices without magnetized electrodes. This large enhancement factor is much greater than all previously reported values for functionalized NW photodetectors. Our results demonstrate a very simple and feasible way to achieve ultrahigh gain photodetectors; these devices can be included in many other systems and represent a new avenue for the creation of high-efficiency optoelectronic devices based on the coupling between ferromagnetic materials and nanostructured semiconductors.

ACKNOWLEDGEMENTS

This work is supported by grants from the National Science Council and Ministry of Education of the Republic of China. We thank Professor Liang for supporting the transmission electron microscopy image.

- 1 Prinz, G. A. Hybrid ferromagnetic-semiconductor structures. *Science* **250**, 1092–1097 (1990).
- 2 Jungwirth, T., Wunderlich, J. & Olejnik, K. Spin Hall effect devices. *Nat. Mater.* **11**, 382–390 (2012).
- 3 Zwanenburg, F. A., van der Mast, D. W., Heersche, H. B., Kouwenhoven, L. P. & Bakkers, E. Electric field control of magnetoresistance in InP nanowires with ferromagnetic contacts. *Nano Lett.* **9**, 2704–2709 (2009).
- 4 Xie, P., Xiong, Q. H., Fang, Y., Qing, Q. & Lieber, C. M. Local electrical potential detection of DNA by nanowire-nanopore sensors. *Nat. Nanotechnol.* **7**, 119–125 (2012).
- 5 Yan, H., Choe, H. S., Nam, S. W., Hu, Y. J., Das, S., Klemic, J. F., Ellenbogen, J. C. & Lieber, C. M. Programmable nanowire circuits for nanoprocessors. *Nature* **470**, 240–244 (2011).
- 6 Varghese, B., Hoong, T. C., Yanwu, Z., Reddy, M. V., Chowdari, B. V. R., Wee, A. T. S., Vincent, T. B. C., Lim, C. T. & Sow, C. H. Co₃O₄ nanostructures with different morphologies and their field-emission properties. *Adv. Funct. Mater.* **17**, 1932–1939 (2007).
- 7 Fang, X. S., Yan, J., Hu, L. F., Liu, H. & Lee, P. S. Thin SnO₂ nanowires with uniform diameter as excellent field emitters: a stability of more than 2400 minutes. *Adv. Funct. Mater.* **22**, 1613–1622 (2012).
- 8 Bie, Y. Q., Liao, Z. M., Zhang, H. Z., Li, G. R., Ye, Y., Zhou, Y. B., Xu, J., Qin, Z. X., Dai, L. & Yu, D. P. Self-powered, ultrafast, visible-blind UV detection and optical logical operation based on ZnO/Ga nanoscale p-n junctions. *Adv. Mater.* **23**, 649–653 (2011).
- 9 Rigutti, L., Tchernycheva, M., Bugallo, A. D., Jacquin, G., Julien, F. H., Zagone, L. F., March, K., Stephan, O., Kociak, M. & Songmuang, R. Ultraviolet photodetector based on GaN/AlN quantum discs in a single nanowire. *Nano Lett.* **10**, 4284–4284 (2010).
- 10 Tang, J. S., Wang, C. Y., Xiu, F. X., Lang, M. R., Chu, L. W., Tsai, C. J., Chueh, Y. L., Chen, L. J. & Wang, K. L. Oxide-confined formation of germanium nanowire heterostructures for high-performance transistors. *ACS Nano* **5**, 6008–6015 (2011).
- 11 Kulmala, T. S., Colli, A., Fasoli, A., Lombardo, A., Haque, S. & Ferrari, A. C. Self-aligned coupled nanowire transistor. *ACS Nano* **5**, 6910–6915 (2011).
- 12 Krishnamoorthy, T., Tang, M. Z., Verma, A., Nair, A. S., Pliszka, D., Mhaisalkar, S. G. & Ramakrishna, S. A facile route to vertically aligned electrospun SnO₂ nanowires on a transparent conducting oxide substrate for dye-sensitized solar cells. *J. Mater. Chem.* **22**, 2166–2172 (2012).
- 13 Lin, C. H., Chen, R. S., Chen, T. T., Chen, H. Y., Chen, Y. F., Chen, K. H. & Chen, L. C. High photocurrent gain in SnO₂ nanowires. *Appl. Phys. Lett.* **93**, 112115 (2008).
- 14 Snaith, H. J. & Ducati, C. SnO₂-based dye-sensitized hybrid solar cells exhibiting near unity absorbed photon-to-electron conversion efficiency. *Nano Lett.* **10**, 1259–1265 (2010).
- 15 Kim, J., Yun, J. H., Kim, C. H., Park, Y. C., Woo, J. Y., Park, J., Lee, J. H., Yi, J. & Han, C. S. ZnO nanowire-embedded Schottky diode for effective UV detection by the barrier reduction effect. *Nanotechnology* **21**, 115205 (2010).
- 16 Soci, C., Zhang, A., Xiang, B., Dayeh, S. A., Aplin, D. P. R., Park, J., Bao, X. Y., Lo, Y. H. & Wang, D. ZnO nanowire UV photodetectors with high internal gain. *Nano Lett.* **7**, 1003–1009 (2007).
- 17 Prades, J. D., Hernandez-Ramirez, F., Jimenez-Diaz, R., Manzanares, M., Andreu, T., Cirera, A., Romano-Rodriguez, A. & Morante, J. R. The effects of electron-hole separation on the photoconductivity of individual metal oxide nanowires. *Nanotechnology* **19**, 465501 (2008).
- 18 Kolmakov, A., Zhang, Y. X., Cheng, G. S. & Moskovits, M. Detection of CO and O₂ using tin oxide nanowire sensors. *Adv. Mater.* **15**, 997–1000 (2003).
- 19 Choi, Y. J., Hwang, I. S., Park, J. G., Choi, K. J., Park, J. H. & Lee, J. H. Novel fabrication of an SnO₂ nanowire gas sensor with high sensitivity. *Nanotechnology* **19**, 095508 (2008).
- 20 Kolmakov, A., Klenov, D. O., Lilach, Y., Stemmer, S. & Moskovits, M. Enhanced gas sensing by individual SnO₂ nanowires and nanobelts functionalized with Pd catalyst particles. *Nano Lett.* **5**, 667–673 (2005).
- 21 Chen, X. H. & Moskovits, M. Observing catalysis through the agency of the participating electrons: Surface-chemistry-induced current changes in a tin oxide nanowire decorated with silver. *Nano Lett.* **7**, 807–812 (2007).
- 22 Lin, C. H., Chen, T. T. & Chen, Y. F. Photocurrent enhancement of SnO₂ nanowires through Au-nanoparticles decoration. *Opt. Express* **16**, 16916–16922 (2008).
- 23 Lu, M. L., Lin, T. Y., Weng, T. M. & Chen, Y. F. Large enhancement of photocurrent gain based on the composite of a single n-type SnO₂ nanowire and p-type NiO nanoparticles. *Opt. Express* **19**, 16266–16272 (2011).
- 24 Lu, M. L., Lin, C. H. & Chen, Y. F. Enhanced photocurrent gain and spectrum range based on the composite consisting of SnO₂ nanowires and CdSe quantum dots. *Appl. Phys. Lett.* **99**, 081109 (2011).
- 25 Yang, H. Y., Yu, S. F., Lau, S. P., Tsang, S. H., Xing, G. Z. & Wu, T. Ultraviolet coherent random lasing in randomly assembled SnO₂ nanowires. *Appl. Phys. Lett.* **94**, 241121 (2009).
- 26 Yang, Q., Guo, X., Wang, W. H., Zhang, Y., Xu, S., Lien, D. H. & Wang, Z. L. Enhancing sensitivity of a single ZnO micro-/nanowire photodetector by piezo-phototronic effect. *ACS Nano* **4**, 6285–6291 (2010).
- 27 Chen, M. W., Chen, C. Y., Lien, D. H., Ding, Y. & He, J. H. Photoconductive enhancement of single ZnO nanowire through localized Schottky effects. *Opt. Express* **18**, 14836–14841 (2010).
- 28 Zhou, W., Liu, R., Wan, Q., Zhang, Q., Pan, A., Guo, L. & Zou, B. Bound exciton and optical properties of SnO₂ one-dimensional nanostructures. *J. Phys. Chem. C* **113**, 1719–1726 (2009).
- 29 Binet, F., Duboz, J. Y., Rosencher, E., Scholz, F. & Harle, V. Mechanisms of recombination in GaN photodetectors. *Appl. Phys. Lett.* **69**, 1202–1204 (1996).
- 30 Muñoz, E., Monroy, E., Garrido, J. A., Izpura, I., Sanchez, F. J., SanchezGarcia, M. A., Calleja, E., Beaumont, B. & Gibart, P. Photoconductor gain mechanisms in GaN ultraviolet detectors. *Appl. Phys. Lett.* **71**, 870–872 (1997).
- 31 Wang, Y., Ramos, I. & Santiago-Aviles, J. J. Optical bandgap and photoconductance of electrospun tin oxide nanofibers. *J. Appl. Phys.* **102**, 093517 (2007).
- 32 Zhou, X. T., Heigl, F., Murphy, M. W., Sham, T. K., Regier, T., Coulthard, I. & Blyth, R. I. R. Time-resolved X-ray excited optical luminescence from SnO₂ nanoribbons: direct evidence for the origin of the blue luminescence and the role of surface states. *Appl. Phys. Lett.* **89**, 213109 (2006).
- 33 Garrido, J. A., Monroy, E., Izpura, I. & Munoz, E. Photoconductive gain modelling of GaN photoconductors. *Semicond. Sci. Technol.* **13**, 563–568 (1998).
- 34 Wu, T., Bur, A., Hockel, J. L., Wong, K., Chung, T. K. & Carman, G. P. Electrical and mechanical manipulation of ferromagnetic properties in polycrystalline nickel thin film. *IEEE Magn. Lett.* **2**, 6000104 (2011).
- 35 Rattanasakulthong, W., Sirisangawang, P., Pinitsoontorn, S. & Sirisathitkul, C. Dependence of hysteresis loops on thickness of thin nickel films prepared by RF sputtering. *Adv. Mat. Res.* **335-336**, 1443–1447 (2011).
- 36 Hernandez-Ramirez, F., Prades, J. D., Tarancón, A., Barth, S., Casals, O., Jimenez-Diaz, R., Pellicer, E., Rodriguez, J., Morante, J. R., Juli, M. A., Mathur, S. & Romano-Rodriguez, A. Insight into the role of oxygen diffusion in the sensing mechanisms of SnO₂ nanowires. *Adv. Funct. Mater.* **18**, 2990–2994 (2008).
- 37 Maier, J. & Gopal, W. Investigations of the bulk defect chemistry of polycrystalline talline tin (IV) oxide. *J. Solid State Chem.* **72**, 293–302 (1988).
- 38 Chen, R. S., Chen, H. Y., Lu, C. Y., Chen, K. H., Chen, C. P., Chen, L. C. & Yang, Y. J. Ultrahigh photocurrent gain in m-axial GaN nanowires. *Appl. Phys. Lett.* **91**, 223106 (2007).
- 39 Hu, L. F., Yan, J., Liao, M. Y., Wu, L. M. & Fang, X. S. Ultrahigh external quantum efficiency from thin SnO₂ nanowire ultraviolet photodetectors. *Small* **7**, 1012–1017 (2011).



This work is licensed under the Creative Commons Attribution-NonCommercial-No Derivative Works 3.0 Unported License. To view a copy of this license, visit <http://creativecommons.org/licenses/by-nc-nd/3.0/>